J Mater Sci (2006) 41:5718–5722
DOI 10.1007/s10853-006-0097-5

LETTER

A technique for characterizing spatial distributions of particles based on *N*th-nearest neighbor statistics

Jeremy W. Leggoe

Received: 19 February 2005 / Accepted: 11 October 2005 / Published online: 16 May 2006

Spatial heterogeneity in secondary phase particle distributions can strongly influence failure processes. In developing models that capture the stochastic nature of failure, the fact that real particle distributions rarely exhibit the ''true'' randomness of an equilibrium ensemble (as may be generated computationally using a Metropolis algorithm [1]) presents a challenge. In modeling investigations, some form of ''random'' state has typically been assumed. Representative volume element models are often employed in which particles are added via Random Sequential Addition (RSA) [2–5]. Microstructures that deviate from equilibrium have been modeled by distributing particles within randomly dispersed spherical clusters [6], or by adopting a cellular automata approach [7–9]; in each case, the model microstructures were arbitrarily constructed.

Enhancing the fidelity of multiphase material models requires the construction of models that recreate the true spatial statistics of real materials. Disordered heterogeneous materials may be reconstructed using an ''energy minimization'' technique based on correlations such as the radial distribution function [10–14]. An initial microstructure is allowed to evolve towards exhibiting the desired correlation function via a Metropolis approach [15]; the probability of a particle move being accepted is based on an ''energy'' representing the difference between the current and target correlation functions. The two-particle radial distribution function is, however, not well suited to reconstructing microstructures exhibiting significant particle clustering [9], necessitating identification of a correlation that characterizes the extent and severity of clustering.

The mean center-to-center distance to the 1st nearest neighbor particle ($\langle L_N \rangle$) is well established as a tool for qualitatively characterizing deviation from a ''random'' state [16–19]. Dirichlet tessellation of two-dimensional particle distributions can extend the characterization to include the first shell of ''near'' neighbor particles, through measures such as the mean ''near'' neighbor distance, the coefficient of variation in the near neighbor distance, and the cell area fraction [20, 21].

Clustering may, however, extend much further than the first shell of near neighbors. Comparing the mean center-to-center distance to the *N*th-nearest neighbor particle in an actual microstructure ($\langle L_N \rangle$) with the value expected for an equilibrium particle distribution ($\langle R_N \rangle$), an approach originally proposed to quantify deviation from a Poisson point process in plant populations [22, 23], provides a means of qualitatively and quantitatively characterizing deviation from equilibrium. The ''deviation ratio'' Δ_N may be defined as

$$\Delta_N = \frac{\langle L_N \rangle}{\langle R_N \rangle} \tag{1}$$

For generality, $\langle L_N \rangle$ and $\langle R_N \rangle$ must be normalized by the mean particle diameter. For distributions in which clustering is more severe than expected at equilibrium, $\Delta_N < 1$; $\Delta_N > 1$ or oscillations in Δ_N would indicate the presence of local order in the distribution. With increasing *N*, the effects of short range clustering or ordering should diminish, and the ratio should tend towards one.

In characterizing particle distributions, the source of the $\langle R_N \rangle$ data must be selected in accordance with the nature of the data available. In many instances, the particle distribution

J. W. Leggoe (✉)
Department of Chemical Engineering, Texas Tech University,
P.O. Box 43121, Lubbock, Texas 79409-3121, USA
e-mail: Jeremy.Leggoe@coe.ttu.edu

data will be compiled from two-dimensional micrographs. For a two-dimensional point process, the mean distance to the *N*th-nearest neighbor point ($\langle P_N \rangle$) is given by [22]

$$\langle P_N \rangle = \frac{N.(2N)!}{(2^n N!)^2 \lambda^{1/2}} \quad (2)$$

where λ is the intensity (number of points per unit area). Testing of the ''randomness'' of particle distributions has often been based on values of P_1 calculated using Eq. 2 [16–19].

Spatial distributions of impenetrable particles, however, constitute ''inhibited'' point processes. While formulae have been derived that place bounds on $\langle R_1 \rangle$ for equilibrium ensembles of monodisperse particles in two- and three-dimensions [1], exact analytical expressions are not available for higher order neighbors. Computer simulations have been undertaken to secure $\langle R_N \rangle$ for N up to 20 for equilibrium ensembles of monodisperse particles in two and three dimensions, and equations have been established to predict $\langle R_N \rangle$ for $N \leq 3$ (in 2D) and $N \leq 6$ (in 3D) [24, 25]. The three dimensional results may be used to compute Δ_N if a three-dimensional characterization of the particle distribution is available.

The particle distribution in a micrograph, however, results from taking a slice through a three-dimensional particle array. For a three-dimensional array of monodisperse spheres, the slice contains a polydisperse set of disks having a mean disk diameter of πD/4 (D = sphere diameter). Given that the disk arrangement is governed by three-dimensional exclusion effects, there is no reason to expect that the mean *N*th-nearest neighbor distances would be equivalent to those obtained from a two-dimensional equilibrium ensemble of disks. This is confirmed by Fig. 1, which compares the distances to the *N*th-nearest neighbor for a volume fraction of 0.20 for (a) a three-dimensional equilibrium ensemble of monodisperse spheres of unit diameter [26], (b) a slice through an equivalent ensemble, and (c) a two-dimensional array of monodisperse disks of diameter $\pi/4$ (matching the mean diameter of the disks on the slice).

Since the current investigation considers spatial distribution data drawn from micrographs, computation of the deviation ratio must be based on the $\langle R_N \rangle$ obtained for slices through three-dimensional equilibrium ensembles of monodisperse spheres. To fully evaluate the extent of clustering, and understand the manner in which the $\langle R_N \rangle$ of an inhibited point process tend towards the $\langle P_N \rangle$ of the point process with increasing N, for this investigation the $\langle R_N \rangle$ needed to be computed for $N \leq 200$ for sphere volume fractions of 0.10 and 0.20.

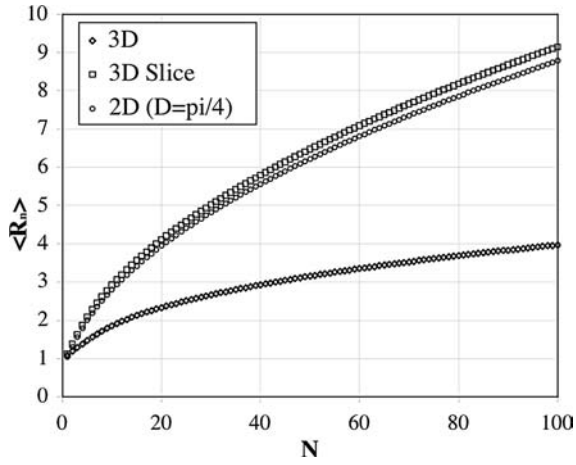

Fig. 1 Plot of the distances to the *N*th-nearest neighbor for a volume fraction of 0.20 for (**a**) a three-dimensional equilibrium ensemble of monodisperse spheres of unit diameter [26], (**b**) a slice through an equivalent ensemble, and (**c**) a two-dimensional equilibrium ensemble of monodisperse disks of diameter $\pi/4$ (matching the mean diameter of the disks on the slice)

To accomplish this, initial particle arrays were created using RSA to place 10000 spheres of unit diameter within a right parallelepiped sized to both achieve the desired volume fraction exactly and ensure that slices aligned with the *XY*-plane intersected enough particles to yield valid statistics for $N \leq 200$. The particles were then moved randomly using a Metropolis algorithm, the mean move distance being adjusted to achieve a 50% probability of acceptance. Particles leaving the volume reappeared periodically at the opposite face of the volume. When assessing the permissibility of a move, edge effects were accounted for by constructing a ''periodic torus'' of periodic image volumes surrounding the base volume.

For each volume fraction, the first 400 realizations were ignored to allow equilibrium to be achieved; every 20th realization thereafter was stored for sampling until a total of 100 realizations had been stored. Five slices sampling the full depth were made through each stored realization. Edge effects were accounted for when computing *N*th-nearest neighbor distances by creating a two dimensional periodic torus surrounding the base realization. The normalized *N*th-nearest neighbor distances (R_N divided by the particle diameter) for every sliced particle were then stored for statistical computations.

The ''inhibition ratio'' ρ_N may be defined as the ratio of the mean center-center distance to the *N*th-nearest neighbor for a slice to the mean distance to the *N*th-nearest neighbor for a point process of equivalent intensity;

$$\rho_N = \frac{\langle R_N \rangle}{\langle P_N \rangle} \quad (3)$$

The inhibition ratio is plotted as a function of N for both volume fractions in Fig. 2. The inhibition effect is significant (ρ_N is greater than 1.005) for $N \leq 28$ (for 0.10 volume fraction) and $N \leq 60$ (0.20); thereafter $\rho_N \cong 1$. Some oscillation in ρ_N due to short-range packing has been observed at high area/volume fractions for monodisperse disks and spheres [24–26]; for the volume fractions under consideration, any oscillation in the slice data was negligible.

To illustrate the performance of the deviation ratio approach, the results obtained for two idealized model systems created by RSA are presented in Fig. 3. For both model systems, 100 realizations were created in which 10000 monodisperse spheres were distributed within cubic volumes sized to achieve a volume fraction of 0.10. Ten slices were then passed through each realization, and the deviation ratio was computed by comparing the mean Nth-nearest neighbor distances for the slices through the model systems with the distances expected for slices through equilibrium ensembles of monodisperse spheres of the same volume fraction.

For the first system, sphere centers were not permitted to approach closer than 1.25 times the sphere diameter, creating an artificially large exclusion zone. For this system the deviation ratio was greater than unity for all values of N. There was significant deviation from the equilibrium statistics for $N < 4$, indicating that this exclusion zone affected nearest neighbor distances only over a relatively limited range. For the second model system, spheres were placed within spherical clusters, with each cluster containing 20 particles. 500 ''cluster spheres'' were placed within the volume by RSA, and then 20 particles were placed within each cluster sphere by RSA. The volume fraction within each individual cluster was approximately 0.20. The resulting deviation ratios were less than unity for all N, with the ratio providing evidence of significant clustering for values of $N < 12$.

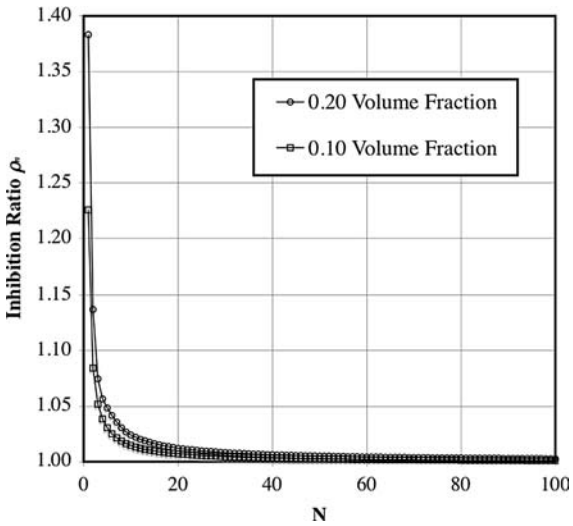

Fig. 2 Plot of the inhibition ratio for slices through three-dimensional equilibrium ensembles of monodisperse spheres at volume fractions of 0.1 and 0.2

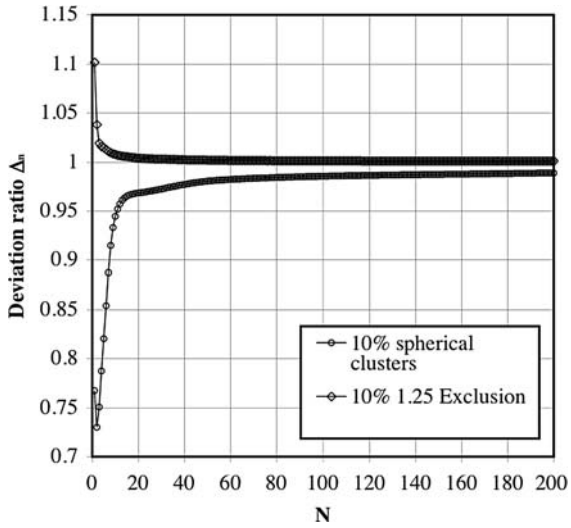

Fig. 3 Deviation ratios plotted as a function of N for two idealized 0.10 volume fraction model systems created by RSA. For the spherical cluster system, 20 particles were placed by RSA within each of 500 spheres that were themselves placed by RSA. For the ''1.25 exclusion'' system sphere centers were prohibited from approaching closer than 1.25 times the sphere diameter

Given that each spherical cluster originally contained 20 particles, this is consistent with the fact that a slice only samples some portion of the particles within each cluster, and highlights that further work needs to be done to characterize the relationship between the ''slice'' data drawn from micrographs and the characteristics of three-dimensional microstructures. Interestingly, the high local volume fraction within the clusters creates an initial oscillation in the deviation ratio, similar to the shell packing effect observed for three dimensional equilibrium ensembles [26].

The illustrate the behavior of the deviation ratio for a real material system, the distribution of silicon carbide particles in the melt cast Duralcan F3S.20S (aluminium 359 – 0.20 volume fraction SiC) particulate reinforced metal matrix composite (PRMMC) depicted in Fig. 4 was analyzed. The SiC particles are the dark particles in Fig. 4; the light particles are silicon particles formed during the solidification of the silicon-rich casting alloy matrix. The SiC particle distribution exhibits significant clustering due to the interdendritic segregation that arises during solidification.

The $\langle L_N \rangle$ for the SiC particles in the Duralcan F3S.20S PRMMC were computed by analysis of the micrograph in Fig. 4 using NIH Image (version 1.61). The image depicts 605 sliced SiC particles, with the $\langle L_N \rangle$ being obtained by

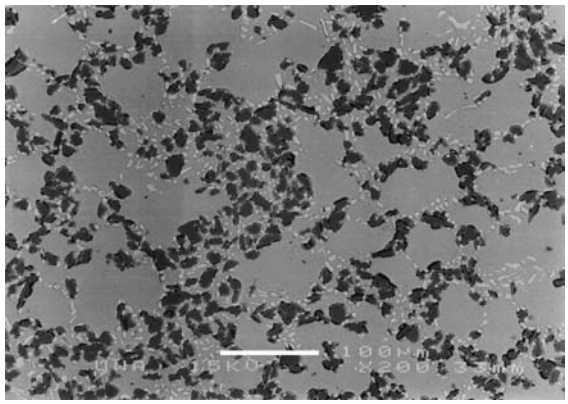

Fig. 4 Back-scattered electron micrograph of a Duralcan F3S.20S PRMMC exhibiting interdendritic segregation. The dark particles are the Silicon Carbide particles considered in this investigation; the light particles are silicon particles formed within the Al 356 matrix. The scale bar is 100 μm long

averaging the results obtained for all SiC particles. Edge effects were again accounted for by creating a periodic torus surrounding the original image. The mean particle diameter was calculated using the Schwarz–Saltykov diameter method [27], yielding an estimated diameter of 12.2 μm.

The deviation ratio values are plotted as a function of N in figure 5. From qualitative inspection of Fig. 5, the clustering appears to extend (in the slice) over the range of 20–25 particles. The variation of Δ_N can be described by an exponential function of the form

$$\Delta_N = 1 - C_1 \exp\left(-C_2 N^{1/3}\right) \tag{4}$$

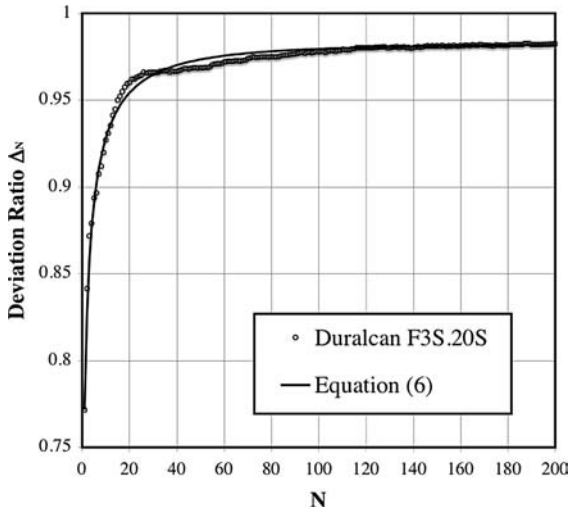

Fig. 5 Deviation ratio plotted as a function of N for the Duralcan F3S.20S PRMMC. A curve fitted to the data using Eq. 6 is also shown, with constants C_1 = 0.681 and C_2 = 1.173

Where C_1 and C_2 are constants determined by curve fitting. The power $N^{1/3}$ was adopted for consistency with the number of particles within a sphere, and was found to give a superior fit than N^1.

An alternate numerical indicator of clustering severity may be defined by adapting a measure of translational order proposed by Torquato et al. [28]. As originally defined, relative ordering was quantified by comparing occupation numbers for a spherical shell of varying diameter with the values expected for ideal and FCC arrangements. In contrast, to quantify the deviation from equilibrium one may define a clustering parameter χ;

$$\chi = \sum_{n=1}^{200} (1 - \Delta_N) \tag{5}$$

Both measures are sensitive to the estimate of the mean particle diameter, which can be highly uncertain for real materials. The function in Eq. 4 is the more robust measure, as its form will be unaffected by the assumed particle diameter; it will simply translate vertically if the assumed diameter is altered, and a valid qualitative estimate of the extent of clustering may still be obtained. In the form proposed in Eq. 5, the χ parameter is obviously sensitive to such a translation. To render both measures more robust in the face of uncertainty in the particle diameter, the constant ''1'' in both equation may be replaced by the value of Δ_{200}, representing the far-field value of Δ_N. The measures may then be rewritten:

$$\Delta_N = \Delta_{200} - C_1 \exp\left(-C_2 N^{1/3}\right) \tag{6}$$

$$\chi = \sum_{n=1}^{200} (\Delta_{200} - \Delta_N) \tag{7}$$

For the Duralcan F3S.20S PR MMC, least squares fitting yields C_1 and C_2 equal to 0.681 and 1.173 respectively (the resulting curve is plotted in Fig. 5); the value of the χ parameter is 2.40.

In its present form, the proposed approach appears to provide a solid foundation for characterizing spatial distributions of particles based on micrograph data. Equations (4) and (6) provide a correlation that may be used for the reconstruction of realistic particle distributions. The value of the χ parameter may be used in conjunction with measures of the range of clustering (such as the range over which the deviation ratio is significantly different from unity) to provide an indication of the relative severity of clustering.

This initial investigation has collected data for slices through equilibrium ensembles of monodisperse spheres of a single volume fraction. It must be remembered, however, that real particle distributions, such as that in the Duralcan F3S.20S PR MMC, are generally comprised of polydisperse non-spherical particles. It has been noted that polydispersity in the particle distribution can increase the mean surface–surface distance for the 1st-nearest neighbor [29]; further investigation is presently underway to determine polydispersity's effect on the inhibition ratio for higher order nearest neighbors, and thus its likely effect on the value of the deviation ratio computed for the Duralcan F3S.20S PR MMC. For non-spherical particles, it will also be necessary to combine correlations based on the deviation ratio with correlations describing the local orientation distribution to generate completely realistic reconstructions. At this time, the fundamental spatial statistical data for equilibrium ensembles of polydisperse and non-spherical particles that are needed to compute deviation ratios and other necessary correlations for real materials have not been reported. Collection of this data is obviously a priority in the continuing development of techniques for characterizing heterogeneity in real materials.

References

1. Torquato S (2002) Random heterogeneous materials – microstructure and macroscopic properties. Springer-Verlag, New York
2. Brockenbrough JT, Suresh S, Wienecke HA (1991) Acta metal Mater 39:735
3. Shen H, Lissenden CJ (2002) Mater Sci Eng A338:2355
4. Gonzalez C, Segurado J, Llorca J (2004) J Mech Phys Solids 52:1573
5. Llorca J, Segurado J (2004) Mater Sci Eng A365:267
6. Segurado J, Gonzalez C, Llorca J (2003) Acta Mater 51:2355
7. Leggoe JW, Mammoli AA, Bush MB, Hu XZ (1998) Acta Mater 46:6075
8. Khvastunkov MS, Leggoe JW (2004) Mater Sci Eng A383:347
9. Khvastunkov MS, Leggoe JW (2004) Scripta Mater 51:309
10. Rintoul MD, Torquato S (1997) J Colloid Interface Sci 186:467
11. Yeong CLY, Torquato S (1998) Phys Rev E 57:495
12. Yeong CLY, Torquato S (1998) Phys Rev E 58:224
13. Cule D, Torquato S (1999) J Appl Phys 86:3428
14. Sheehan N, Torquato S (2001) J Appl Phys 89:53
15. Metropolis N, Rosenbluth AW, Rosenbluth MN, Teller AH, Teller E (1953) J Chem Phys 21:1087
16. Schwarz H, Exner HE (1983) J Microscopy 129:155
17. Vander Voort GF (1991) Mater Char 27:241
18. Zhang J, Przystupa MA, Luevano AJ (1998) Metall Mater Trans A 29:727
19. Anson JP, Gruzleski JE (1999) Mater Char 43:319
20. Murphy AM, Howard SJ, Clyne TW (1988) Mater Sci Technol 14:959
21. Yang N, Boselli J, Sinclair I (2001) J Microscopy 201:189
22. Cressie NAC (1993) Statistics for spatial data. Wiley Interscience, New York
23. Thompson HR (1956) Ecology 37:391
24. Tewari A, Gokhale AM (2004) Comp Mater Sci 31:13
25. Tewari A, Gokhale AM (2004) Mater Sci Eng A 385:332
26. Leggoe JW, and Riggs JB, (2005) Mater Sci Eng A submitted
27. Underwood EE (1970) Quantitative stereology. Addison-Wesley, Reading
28. Torquato S, Truskett TM, Debenedetti PG (2000) Phys Rev Lett 84:2064
29. Lu B, Torquato S (1992) Phys Rev A 45:5530